Small-Signal Modelling and Stability Analysis of Current-Controlled Virtual Synchronous Generators

D W SUN[1,2], H LIU[1,2], P SONG[1,2], S ZHU[3] and Z WEI[4]

[1]State Grid Jibei Electric Power Co. Ltd. Research Institute, Beijing, China
[2] Grid-connected Operation Technology for Wind-Solar-Storage Hybrid System State Grid Corporation Key Laboratory, Beijing, China.
[3]Zhangjiakou Wind and Solar Power Energy Demonstration Station Co. Ltd. Zhangjiakou, China
[4] Nari Solar Energy Technology Co. Ltd., Nanjing, China
E-mail: dddd129216713@126.com

Abstract. Virtual Synchronous Generators (VSG), as an effective mean to improve the frequency and voltage regulation ability of the renewable power, had aroused wide concern. Researchers have proposed several VSG implementations, which can be classified into two categories: voltage-controlled VSG and current-controlled VSG. Voltage-controlled VSG have been extensively studied. However, few researches focused on current-controlled VSG. In this paper, we concentrated on the current-controlled VSG and its stability problem. Firstly, a small-signal model of current-controlled VSG was established to identify the oscillation modes of grid-connected VSG system. Moreover, the developed model was used to investigate damping characteristics of the system under various scenarios and with different control parameters. The results revealed that stability of VSG system was sufficiently impacted by virtual inertia and phase lock loop in VSG. Under some unfavourable conditions, current-controlled VSG would contribute to high-frequency or subsynchronous oscillation.

1. Introduction

Renewable power generators (RPG) based on wind and photovoltaic are developing rapidly in recent years and the percentage of RPG connected to the grid is in growing [1]. As the interface between RPG and the grid, the grid-connected inverter is not able to provide inertia and damping for the power system [2]. The increasing of RPG and grid-connected inverters will cause stability problems in power grid because of the lack of inertia and damping [3]. To solve this problem, virtual synchronous generator (VSG) technology was proposed to control the grid-connected inverter to emulate the essential behaviour of synchronous generators [4], including the droop mechanism and inertial characteristic [5].

Recently, some researches have been conducted on VSG technology. Technical route and stability problem of VSG are two important research directions. For the first direction, existing studies proposed two different technical routes, which are voltage-controlled and current-controlled VSG [6]-[9]. Refer to the stability of VSG, researches concentrated on the risk of oscillation caused by voltage-controlled VSG [10]-[12] discussed the small-signal stability of current-controlled VSG, which was applied in photovoltaic power generator in microgrid. A method was proposed in [13] to improve the oscillation damping by optimizing the control parameters of VSG. This method was designed for voltage-controlled VSG in microgrid. The oscillation mechanism in parallel operations of voltage-controlled VSGs was clarified in [14], which also analysed the influence from parameters of VSG to

oscillation mode. The existing studies mainly concentrated on the stability problem of voltage-controlled VSG. However, the same problem for current-controlled VSG has not been researched.

The analysis of current-controlled VSG stability faced the difficulty of modelling phase lock loop (PLL). The difficulty can be summarized as the following two aspects:

1. There is a big difference between the small-signal model of current-controlled VSG and the model of voltage-controlled VSG. Because voltage-controlled VSG has no PLL, it is not necessary to model PLL [10]-[12]. However, PLL performs an important role in current-controlled VSG. Because PLL has a significant influence on stability of grid-connected current-controlled VSG, it is essential to model the PLL in detail.
2. The model of current-controlled VSG is significantly different from the model of traditional inverter or inverter equipped with droop control [13]. In traditional inverter, PLL provides phase angle to Park transformation [14]. In the inverter equipped with droop control, PLL also sends frequency signal to droop control. However, in current-controlled VSG, PLL not only offers the signal of phase angle and frequency to Park transformation and droop control, but also gives the rate of change of frequency (ROCOF) to the virtual inertia control in VSG. Therefore, the PLL in current-controlled VSG should be modeled accurately.

Besides the above observations, it is worth noting that no prior research on the oscillation problem of current-controlled VSG, which has been adopted in the widely employed grid-connected RPG. To address these issues, this paper investigates the small-signal stability of current-controlled VSG.

The rest of this paper is organized as follows: In Section II, the small-signal model is established for a grid-connected current-controlled VSG system. The damping characteristics of VSG system are analysed in Section III. The developed model is used in Section IV to investigate characteristics of all oscillation modes with control parameters. In Section V, the stability of VSG system is identified under various system scenarios. Finally, brief conclusions are drawn in Section VI.

2. Small-signal model of the VSG

An overview of the studied grid-connected current-controlled VSG system is shown in figure 1, where an inverter is connected to a grid at the point of common coupling (PCC) through an LC filter. R_l, L_l denote the grid impedance at the PCC. The VSG-based inverter control has five functional modules, namely filter processing, PLL, power control, reactive power control and current control.

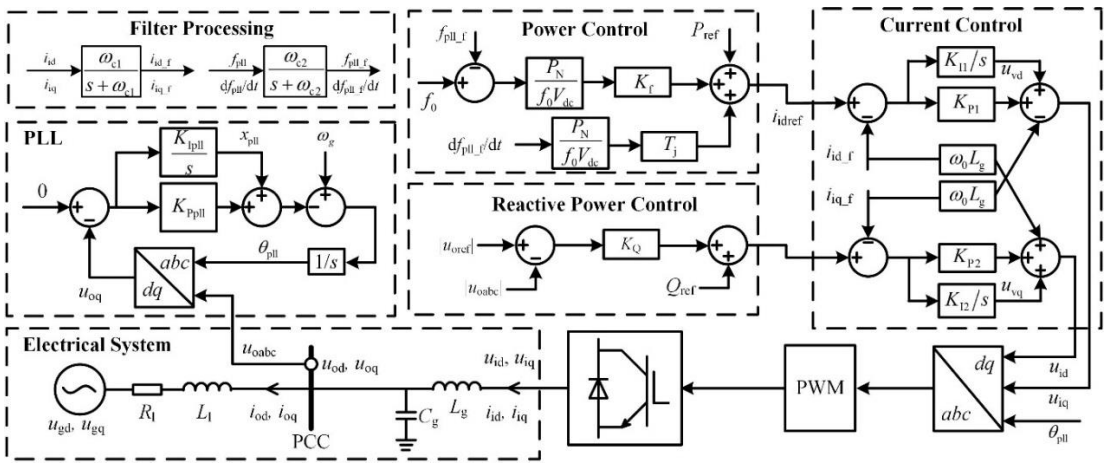

Figure 1. The studied grid-connected current-controlled VSG system

In figure 1, all three phase variables have been transformed into Synchronous Reference Frames (SRFs) based on the amplitude-invariant Park transformation [9]. It is clarified that the entire system is implemented in a SRF defined by the angular position θ_{pll}, which is the phase angle locked by PLL.

2.1. Electrical system

The linearized small-signal model of VSG system can be presented by (1).

$$
\begin{bmatrix}
\mathrm{d}\Delta i_{id}/\mathrm{d}t \\ \mathrm{d}\Delta i_{iq}/\mathrm{d}t \\ \mathrm{d}\Delta u_{od}/\mathrm{d}t \\ \mathrm{d}\Delta u_{oq}/\mathrm{d}t \\ \mathrm{d}\Delta i_{od}/\mathrm{d}t \\ \mathrm{d}\Delta i_{oq}/\mathrm{d}t \\ \mathrm{d}\Delta x_{pll}/\mathrm{d}t \\ \mathrm{d}\Delta\theta_{pll}/\mathrm{d}t \\ \mathrm{d}\Delta i_{id\_f}/\mathrm{d}t \\ \mathrm{d}\Delta i_{iq\_f}/\mathrm{d}t \\ \mathrm{d}\Delta f_{pll\_f}/\mathrm{d}t \\ \mathrm{d}\Delta\left(\mathrm{d}f_{pll\_f}/\mathrm{d}t\right)/\mathrm{d}t \\ \mathrm{d}\Delta u_{vd}/\mathrm{d}t \\ \mathrm{d}\Delta u_{vq}/\mathrm{d}t
\end{bmatrix}
=
\begin{bmatrix}
0 & \omega_g & -\frac{1}{L_g} & 0 & 0 & 0 & 0 & 0 & 0 & 0 & 0 & 0 & 0 & 0 \\
-\omega_g & 0 & 0 & -\frac{1}{L_g} & 0 & 0 & 0 & 0 & 0 & 0 & 0 & 0 & 0 & 0 \\
\frac{1}{C_g} & 0 & -\frac{1}{C_g} & 0 & 0 & \omega_g & 0 & 0 & 0 & 0 & 0 & 0 & 0 & 0 \\
0 & \frac{1}{C_g} & 0 & -\frac{1}{C_g} & -\omega_g & 0 & 0 & 0 & 0 & 0 & 0 & 0 & 0 & 0 \\
0 & 0 & \frac{1}{L_t} & 0 & -\frac{R_t}{L_t} & \omega_g & 0 & \frac{\sin(\theta_{pll0})u_{gd0}}{L_t} & 0 & 0 & 0 & 0 & 0 & 0 \\
0 & 0 & 0 & \frac{1}{L_t} & -\omega_g & -\frac{R_t}{L_t} & 0 & \frac{\cos(\theta_{pll0})u_{gd0}}{L_t} & 0 & 0 & 0 & 0 & 0 & 0 \\
0 & 0 & 0 & -\frac{K_{Ipll}}{V_b} & 0 & 0 & 0 & 0 & 0 & 0 & 0 & 0 & 0 & 0 \\
0 & 0 & 0 & \frac{K_{Ppll}}{V_b} & 0 & 0 & -1 & 0 & 0 & 0 & 0 & 0 & 0 & 0 \\
\frac{\omega_{c1}}{I_b} & 0 & 0 & 0 & 0 & 0 & 0 & 0 & -\omega_{c1} & 0 & 0 & 0 & 0 & 0 \\
0 & \frac{\omega_{c1}}{I_b} & 0 & 0 & 0 & 0 & 0 & 0 & 0 & -\omega_{c1} & 0 & 0 & 0 & 0 \\
0 & 0 & 0 & \frac{K_{Ppll}\omega_{c2}}{2\pi V_b} & 0 & 0 & -\frac{\omega_{c2}}{2\pi} & 0 & 0 & 0 & -\omega_{c2} & 0 & 0 & 0 \\
0 & \frac{K_{Ppll}\omega_{c2}}{2\pi V_b C_g} & -\frac{K_{Ppll}\omega_{c2}\omega_g}{2\pi V_b} & \frac{K_{Ipll}\omega_{c2}}{2\pi V_b} & 0 & -\frac{K_{Ppll}\omega_{c2}}{2\pi V_b C_g} & 0 & 0 & 0 & 0 & 0 & -\omega_{c2} & 0 & 0 \\
0 & 0 & 0 & 0 & 0 & 0 & 0 & 0 & -K_{I1} & 0 & -\frac{K_{I1}K_f}{f_0} & \frac{K_{I1}T_j}{f_0} & 0 & 0 \\
0 & 0 & 0 & 0 & 0 & 0 & 0 & 0 & 0 & -K_{I2} & 0 & 0 & 0 & 0
\end{bmatrix}
\cdot
\begin{bmatrix}
\Delta i_{id} \\ \Delta i_{iq} \\ \Delta u_{od} \\ \Delta u_{oq} \\ \Delta i_{od} \\ \Delta i_{oq} \\ \Delta x_{pll} \\ \Delta\theta_{pll} \\ \Delta i_{id\_f} \\ \Delta i_{iq\_f} \\ \Delta f_{pll\_f} \\ \Delta\left(\mathrm{d}f_{pll\_f}/\mathrm{d}t\right) \\ \Delta u_{vd} \\ \Delta u_{vq}
\end{bmatrix}
+
\begin{bmatrix}
0 \\ 0 \\ 0 \\ 0 \\ 0 \\ 0 \\ 0 \\ 0 \\ 0 \\ 0 \\ 0 \\ 0 \\ \Delta P_{ref}/P_b \\ 0
\end{bmatrix}
\tag{1}
$$

Where u_{id}, u_{iq}, i_{id} and i_{iq} denote the output voltages and currents of VSG in dq frame; u_{od} and u_{oq} are the voltages of PCC in dq frame. i_{od} and i_{oq} represent the injected grid currents in dq frame; ω_g represents the angular frequency of the grid; u_{gd} and u_{gq} are voltages of ac system in dq frame. x_{pll} is the integrator state of the PI controller in PLL; K_{Ppll} and K_{Ipll} denote the proportion coefficient and integral coefficient in PLL, respectively. i_{id_f} and i_{iq_f} represent the filtered i_{id} and i_{iq}; f_{pll} and $\mathrm{d}f_{pll}/\mathrm{d}t$ are the frequency and ROCOF locked by PLL; f_{pll_f} and $\mathrm{d}f_{pll\_f}/\mathrm{d}t$ denote the filtered f_{pll} and $\mathrm{d}f_{pll}/\mathrm{d}t$; ω_1 and ω_2 are the cut-off frequencies of the applied low pass filters. i_{idref} and i_{iqref} denote the VSG output current references; P_{ref} and Q_{ref} are the power and reactive power references of VSG; K_f and K_D represent the power droop gain and reactive power droop constant respectively; f_0 is the frequency reference (50Hz); V_{dc} is the dc voltage of the inverter; $|u_{oref}|$ and $|u_{oabc}|$ denote the amplitudes of PCC voltage reference and measurement; T_j represents the virtual mechanical time constant. u_{vd} and u_{vq} denote the integrator states of the PI controller in current control; K_{P1}, K_{P2}, K_{I1} and K_{I2} represent the proportion coefficients and integral coefficients in PI controller applied in current control, respectively.

2.2. Model validation

The validity of the small-signal state-space model documented by (1) is verified by comparing its dynamic response to the response of a non-linear simulation model. Both of the models are established based on the parameters listed in table 1. The simulations are carried out with MATLAB/Simulink.

Table 1. Parameters of the studied system

Parameter	Value	Parameter	Value	Parameter	Value	Parameter	Value	Parameter	Value
P_{ref}/kW	500	T_j /s	0.1	ω_{c1}	1000π	Q_{ref}/kVar	0	V_{ref}/V	315
C_g/μF	300	L_l/mH	0.0386	ω_{c2}	20π	K_{Ppll}	10	K_{P1} K_{P2}	0.64
L_g/μH	150	R_l/mΩ	1.212	K_f	20	K_{Ipll}	500	K_{I1} K_{I2}	100

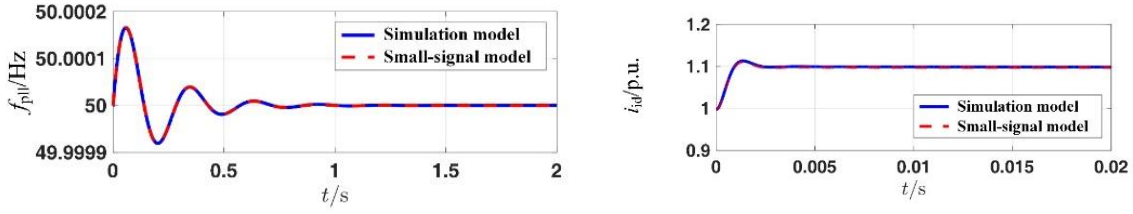

Figure 2. The studied grid-connected current-controlled VSG system

A steady-state point with an active power reference of 1 pu, resulting in i_{id} and f_{pll} equel to 1 pu and 50 Hz respectively, is used for the validation. At time t=0s, the power reference is stepped up to the value of 1.1 pu in both of the small-signal and simulation models. Comparisons of the response obtained with both models are shown in figure 2.
The results of figure 2 clearly show that the i_{id} and f_{pll} of the VSM, which can be calculated from the state variables of the small-signal model, are coinciding with the results from the nonlinear simulation model. Thus, the presented results sufficiently demonstrate that the small-signal model is able to accurately capture the dynamic response of the system.

3. System eigenvalue analysis

Based on the proven small-signal model of VSG, the eigenvalues of the ***A*** matrix can be calculated to systematically identify the oscillation modes and accurately evaluate the stability of VSG system.
Table 2 lists all the system eigenvalues for the steady-state operating point, where the reference values of active and reactive power are set as 1.0 pu and 0. The state variables of highly sensitive to the relevant eigenvalue are also presented in table 2.

Table 2. System eigenvalues

No.	Real part of eigenvalues	Oscillation frequency/Hz	Damping	State variables of highly sensitive
$\lambda_{1\text{-}2}$	**-69.7**	**2873**	**1.7×10^{-4}**	**u_{od}, u_{oq}, i_{od}, i_{oq}**
$\lambda_{3\text{-}4}$	-157.9	2862	3.2×10^{-4}	u_{od}, u_{oq}, i_{od}, i_{oq}
$\lambda_{5\text{-}6}$	-1711.6	400	0.56	i_{id}, i_{iq}, i_{id_f}, i_{iq_f}
$\lambda_{7\text{-}8}$	-1424.1	350	0.54	i_{id}, i_{iq}, i_{id_f}, i_{iq_f}
$\lambda_{9\text{-}10}$	-6.01	0.022	0.99	u_{vd}, u_{vq}
$\lambda_{11\text{-}12}$	-5.01	6.95	0.22	x_{pll}, θ_{pll}
$\lambda_{13\text{-}14}$	-62.84, -62.83	0	1	f_{pll_f}, df_{pll_f}/dt

As shown in table 2, eight oscillation modes were identified corresponding to 14 eigenvalues. All the real parts of eigenvalues are negative, which clarifies that the system is stable with the parameters and operating conditions specified in Table 1. For a further discussion in the oscillation characteristics of VSG system, the poorly damped eigenvalue will be of most interest. From table 2, it can be noticed that $\lambda_{1\text{-}2}$ are the complex conjugate poles of most poorly damp. We placed emphasis on the eigenvalue trajectory of $\lambda_{1\text{-}2}$ in the following sections.

4. Impact of VSG control parameters on stability

For systematically analyzing the impact of VSG control parameters on stability, the parameters are classified into 3 groups: (1) control parameters relevant to VSG function and (2) parameters of PLL. The influence from these three catalogs of parameters are introduced successively in the next subsections.

4.1. Control parameters relevant to VSG function

4.1.1. Virtual mechanical time constant T_j.

The eigenvalue trajectory of the system when sweeping the virtual mechanical time constant T_j from 0.01 to 10 is shown in figure 3.
From figure 3(a), it is observed that $\lambda_{1\text{-}2}$ monotonously move toward the right when T_j increases. The opposite trend appears for $\lambda_{3\text{-}4}$. No such obvious relationship can be found for the other eigenvalues. This observation proves that the oscillatory eigenvalues ($\lambda_{1\text{-}4}$) associated with the LC filter of inverter are strongly influenced by T_j, which directly impacts the damping of high-frequency oscillation mode in the system.
The results from figure 3(b) demonstrates that the damping of oscillation mode corresponding to $\lambda_{1\text{-}2}$ decreases rapidly when T_j increases. When T_j exceeds 0.27s, VSG will produce negative damping that is sufficient to cause unstable high-frequency oscillation.

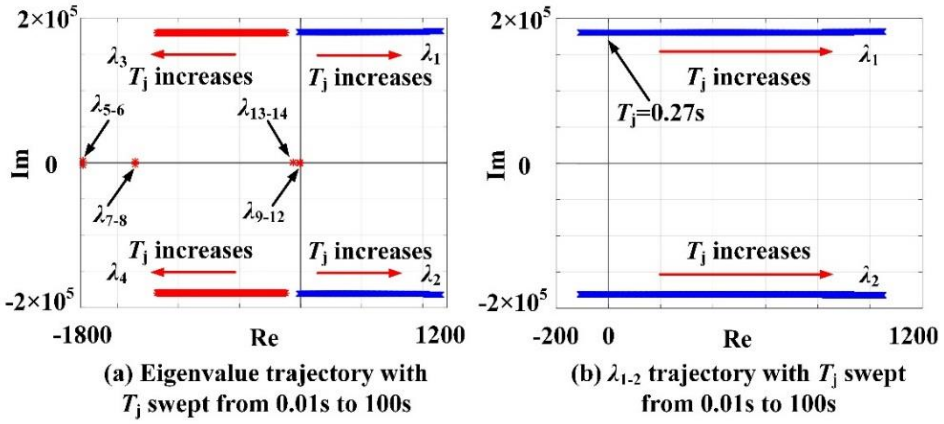

Figure 3. Influence from T_j to eigenvalues

4.1.2. The droop coefficient of power control K_f.

The eigenvalue trajectory with K_f swept from 5 to 20 is given by figure 4.

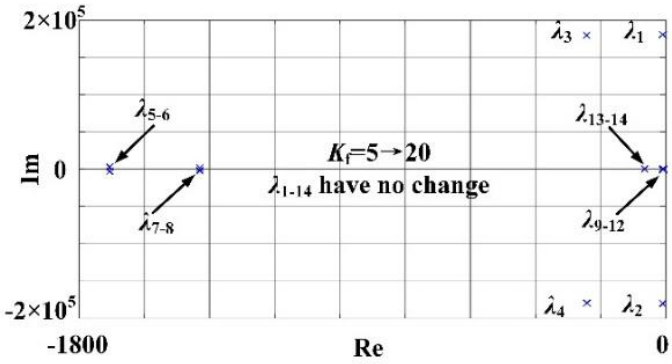

Figure 4. Influence from K_f to eigenvalues

It is obvious that the system eigenvalues have no change in figure 4, which indicates that the change of K_f has little impact on the damping characteristic of VSG system.

From figure 3 and 4, it can be noticed that, T_j has a stronger influence than K_f on VSG system stability. This observation is opposite to that of the voltage-controlled VSG [10]. The diverse impact from T_j and K_f can be explained through the different roles T_j and K_f plays in VSG control. Because ROCOF is considerably larger than frequency difference under small-signal deviation around the point of linearization, T_j, which is corresponding to ROCOF, is more influential than K_f, which is relevant to frequency difference.

4.2. Parameters of PLL

4.2.1. Proportion coefficients of PLL K_{Ppll}.

The eigenvalue trajectory of the system when sweeping the proportion coefficients of PLL K_{Ppll} from 1 to 100 is shown in figure 5.

From figure 5(a), it can be seen that $\lambda_{1\text{-}2}$ move toward the right as K_{Ppll} increases. In contrast, $\lambda_{3\text{-}4}$ and $\lambda_{13\text{-}14}$ move to the left. The other eigenvalues are insensitive to the change of K_{Ppll}.

Figure 5(b) indicates that the damping of oscillation mode corresponding to $\lambda_{1\text{-}2}$ declines when K_{Ppll} increases. Unstable high-frequency oscillation will appear in VSG system when K_{Ppll} exceeds 26.

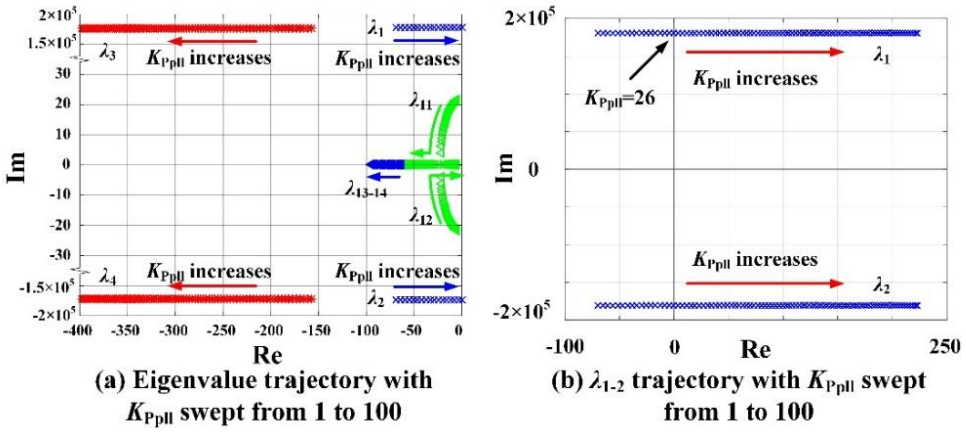

Figure 5. Influence from K_{PpII} to eigenvalues

4.2.2. Integral coefficients of PLL K_{Ipll}.

The eigenvalue trajectory of the system when sweeping the proportion coefficients of PLL K_{IpII} from 500 to 1 is shown in figure 6.

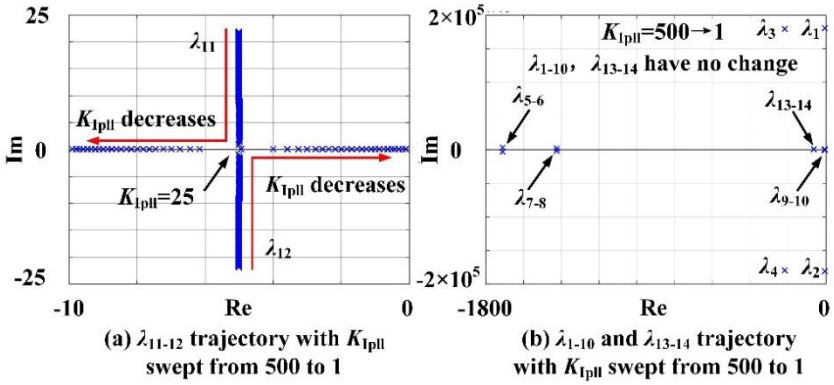

Figure 6. Influence from K_{IpII} to eigenvalues

From figure 7(a), it can be noted that $\lambda_{11\text{-}12}$ move toward the x-axis as K_{IpII} grows initially. When K_{IpII} is above 25, λ_{12} begins to move toward the origin, but will not go over y-axis.

Figure 7(b) illustrates that, except for $\lambda_{11\text{-}12}$, the system eigenvalues have no change, which indicates that the change of K_{IpII} has rare influence on the stability of VSG system.

5. Adaptation of VSG to various grid conditions

For systematically analyzing the adaptation of current-controlled VSG, the damping characteristics of VSG system are investigated under various conditions, for instance, different voltage levels and grid impedances.

5.1. Impact of voltage level on stability

As the ratio of ac grid resistance (R_l) and reactance (X_l) in figure 1, $r_{R/X}$ is defined by (2).

$$r_{R/X} = R_l / X_l = R_l / \left(L_l \times 100 \times \pi\right) \tag{2}$$

Where L_l denote grid inductance.

The value of $r_{R/X}$ can reflect the voltage level of ac system because a smaller $r_{R/X}$ will accordingly appear in a higher voltage power grid. Corresponding to voltage levels of 10kV and 500kV, the typical values of $r_{R/X}$ are 6 and 0.1 respectively. For studying the system stability under most kinds of voltage levels, the eigenvalue trajectory when sweeping $r_{R/X}$ from 0.1 to 6 is shown in figure 8.

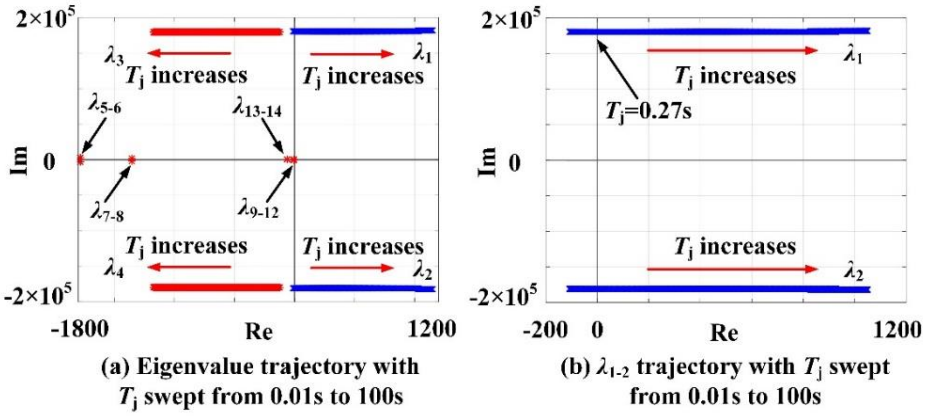

Figure 7. Influence from T_j to eigenvalues

From figure 7, it is observed that $\lambda_{1\text{-}4}$ monotonously move toward the right when $r_{R/X}$ decreases. The other eigenvalues are insensitive to the change of $r_{R/X}$. This observation can be explained by that the real parts of $\lambda_{1\text{-}4}$ are closely relevant to damping characteristic of the connected ac system. The reducing of $r_{R/X}$ will diminish the grid resistance, which develops a negative effect on the damping characteristic.

Therefore, the stability margin will be negatively affected when current-controlled VSG is connected to a high voltage power grid whose $r_{R/X}$ is relatively small. However, it should be noticed that RPG equipped with VSG control will not operate in parallel with the high voltage power grid in most cases. Hence, the instability caused by $r_{R/X}$ is not an important problem for applying current-controlled VSG.

5.2. Impact of grid impedance on stability

The grid impedance Z_L is defined by (3).

$$Z_L = S_b \sqrt{R_l^2 + X_l^2} / \left(V_b\right)^2 \tag{3}$$

Where S_b=500kVA and V_b=315V respectively represent the rated power and voltage of VSG.

The eigenvalue trajectory of VSG system when sweeping Z_L from 0.01pu to 6pu is shown in figure 8.

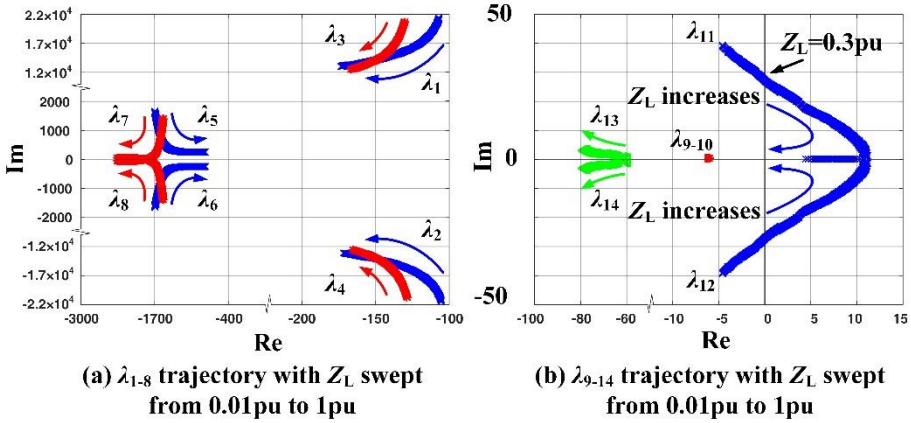

Figure 8. Influence from Z_L to eigenvalues

From figure 8(a), it can be seen that eigenvalues associated with high-frequency oscillation modes stay in the left half plane as Z_L swept from 0.01pu to 1pu, which indicates that the damping of the high-frequency mode is positive. Figure 8(b) indicates that the damping of oscillation mode corresponding to $\lambda_{11\text{-}12}$ declines when Z_L increases. Unstable subsynchronous oscillation will appear in VSG system when Z_L exceeds 0.3pu, which indicates that it may destabilize the whole system by connecting current-controlled VSG to weak power grid.

6. Conclusion

This paper investigates the stability of grid-connected current-controlled VSG system. A small-signal model of the VSG system is developed to quantify the modal damping and it is affected by VSG control parameters. The adaptation of VSG to various grid conditions has also been identified. The following conclusions can be drawn:

1. Oscillation mode of current-controlled VSG system: No oscillation mode will be brought in by introduction of VSG function into traditional inverters, which, however, will have a negative effect on the damping of high-frequency oscillation mode associated with the LC filter of inverter.
2. Impact of VSG control parameters on stability: VSG would contribute to negative damping under some unfavourable conditions, for instance, improper selection of VSG control parameters such as virtual mechanical time constant and proportion coefficients of PLL. In the worst cases of lower electrical and mechanical damping, the high-frequency oscillation mode of VSG system would be marginally stable or even cause sustained oscillation.
3. Adaptation of VSG to various grid conditions: The subsynchronous oscillation will be excited when current-control VSG is connected to a weak power grid, which may result in instability of the system.

This paper focus on the stability of current-controlled VSG when VSG is connected to infinite bus. However, it is also significant to research on the stability of grid-connected current-controlled VSG system under the scenarios of high permeability of renewable power generation, which is the future work and beyond the scope of this paper.

7. References

[1] Sun D, Xie X, Liu Y, et al. Investigation of SSTI Between Practical MMC-based VSC-HVDC and Adjacent Turbogenerators through Modal Signal Injection Test[J]. IEEE Transactions on Power Delivery, 2016, PP (99):1-1.
[2] Sun D, Xie X, Wang J, et al. Integrated generation-transmission expansion planning for offshore oilfield power systems based on genetic Tabu hybrid algorithm [J]. Journal of Modern Power Systems & Clean Energy, 2017, 5(1):117-125.
[3] Sakimoto K, Miura Y, Ise T. Stabilization of a power system including inverter-type distributed generators by a virtual synchronous generator [J]. Electrical Engineering in Japan, 2014, 187 (3): 7-17.
[4] Zhong Q C, Hornik T. Control of Power inverters in renewable energy and smart grid integration [M]. NewYork: Wiley-IEEE Press, 2013.
[5] Li Heming, Zhang Xiangyu, Wang Yi, Zhu Xiaorong. Virtual inertia control of DFIG-based wind turbines based on the optimal power tracking [J]. Proceedings of the CSEE, 2012, 32(7):32-39.
[6] Lv Zhipeng, Sheng Wanxing, Zhong Qingchang, et al. Virtual synchronous generator and its applications in micro-grid [J]. Proceedings of the CSEE, 2014, 34(16): 2591-2603.
[7] D'Arco S, Suul J A. Virtual synchronous machines-Classification of implementations and analysis of equivalence to droop controllers for microgrids [C]. IEEE PowerTech Grenoble, Grenoble, France: IEEE, 2013:1-7.
[8] He J, Li Y W, Guerrero J M, et al. An Islanding Microgrid Power Sharing Approach Using Enhanced Virtual Impedance Control Scheme [J]. IEEE Transactions on Power Electronics, 2013, 28(11):5272-5282.
[9] Z Tianwen, C Laijun, C Tianyi,et al. Review and Prospect of Virtual Synchronous Generator Technologies [J]. Automation of Electric Power Systems, 2015, (21): 165-175.
[10] Yan Xiangwu, Liu Zhengnan, Xu Hengbo, et al. Small-signal modeling and analysis of three-phase characteristics of virtual synchronous generator [J]. Journal of North China Electric Power University, 2016, 43(3): 1-8.
[11] Xie Lingling Shi Bin, Hua Guoyu, et al. Parallel Operation Technology of Distributed Generations Based on Improved Droop Control [J]. Power System Technology, 2013, 4: 992-998.

[12] Zhong Q C. Robust Droop Controller for Accurate Proportional Load Sharing Among Inverters Operated in Parallel [J]. IEEE Transactions on Industrial Electronics, 2012, 60(4):1281-1290.
[13] Soni N, Doolla S, Chandorkar M C. Improvement of Transient Response in Microgrids Using Virtual Inertia [J]. IEEE Transactions on Power Delivery, 2013, 28(3):1830-1838.
[14] Bevrani H, Ise T, Miura Y. Virtual synchronous generators: a survey and new perspective [J], International Journal of Electrical Power and Energy Systems, 2014(54): 244-254.

Acknowledgments
The work of this paper was supported by the projects “research on application technology and grid connection adaptability of renewable power generators equipped with actively supporting ability (52010118000N)” and “research on transmission network planning of renewable power generation convergence area by considering large-scale wind power virtual synchronous generator (52018K180002)”.